Drift-Kinetic Alfvén Waves Observed near a Reconnection X Line in the Earth's Magnetopause

C. C. Chaston,[1] T. D. Phan,[1] J. W. Bonnell,[1] F. S. Mozer,[1] M. Acuña,[2] M. L. Goldstein,[2] A. Balogh,[3] M. Andre,[4] H. Reme,[5] and A. Fazakerley[6]

[1]*Space Science Laboratory, University of California, Berkeley, California 94720, USA*
[2]*NASA Goddard Space Flight Center, Greenbelt, Maryland, USA*
[3]*Imperial College, London, United Kingdom*
[4]*Swedish Institute of Space Physics, Uppsala, Sweden*
[5]*CESR, Toulouse, France*
[6]*Mullard Space Science Laboratory, Dorking, United Kingdom*

(Received 26 January 2005; published 4 August 2005)

We identify drift-kinetic Alfvén waves in the vicinity of a reconnection X line on the Earth's magnetopause. The dispersive properties of these waves have been determined using wavelet interferometric techniques applied to multipoint observations from the Cluster spacecraft. Comparison of the observed wave dispersion with that expected for drift-kinetic Alfvén waves shows close agreement. The waves propagate outwards from the X line suggesting that reconnection is a kinetic Alfvén wave source. Energetic O^+ ions observed in these waves indicate that reconnection is a driver of auroral ion outflow.

DOI: 10.1103/PhysRevLett.95.065002 PACS numbers: 94.30.Tz, 52.35.Kt, 94.30.Va, 95.75.Kk

Alfvén waves are found throughout the solar system [1–4]. At small scales transverse to the background magnetic field these waves are known as kinetic Alfvén waves [5] and may accelerate ions and electrons [6,7]. These waves may be important in coronal heating, the acceleration of the solar wind [8] and the dissipation of solar wind turbulence [9]. Closer to Earth these waves have been shown to drive aurora [10] and induce plasma loss from the ionosphere in the form of outward streaming ions and electrons [11]. However, despite the importance of these waves their source remains unclear. In this Letter we demonstrate that magnetic reconnection is a source for kinetic Alfvén waves using *in situ* measurements from the four Cluster spacecraft [12] separated by ~100 km in the vicinity of the X line.

Figure 1 shows observations from the Cluster 3 spacecraft on 18 March 2002. At this time the satellite was located tailward of the cusp in the northern hemisphere and moving outwards from the magnetosphere and into the magnetosheath. The spacecraft trajectory through the magnetopause and X line is shown schematically in Fig. 1(a). This schematic is based on a previous study of the same event in which reconnection jets and a possible diffusion region were identified from the Walen test and plasma jet reversal respectively [13].

Figure 1(b) shows that the appearance of magnetosheath plasmas provides a ~0.1 ($V_A \approx 10^7$ ms^{-1}, $\beta \approx 0.001$) to ~100 cm^{-3} ($V_A \approx 3.0 \times 10^5$ ms^{-1}, $\beta \geq 1$) density change from 14:55–58 UT across the magnetopause. The largest amplitude electric field oscillations shown in Fig. 1(c) are observed on this density gradient. The largest amplitude magnetic field oscillations, shown in Fig. 1(d), are, however, found in the Earthward directed reconnection jet with an abrupt increase and decrease apparent as the spacecraft enters and exits the jet, respectively. Figure 1(e) shows that the field-aligned wave Poynting flux associated with these electromagnetic waves is directed tailward on the magnetosphere side of the X line and Earthward on the magnetosheath side. Enhancements in electron energy flux shown in Fig. 1(f) occur where large amplitude electromagnetic fluctuations are found and Fig. 1(g) shows that these bursty enhanced fluxes are field-aligned (0°, 180°) and counter-streaming but largely moving anti-Earthward. At the same time Figs. 1(h) and 1(i) show energetic outward streaming (180°) O^+ ions along field lines connecting the ionosphere to the reconnection X line. These ions are observed with the enhanced wave activity and have thermal energies of 8–10 keV or ~4 orders of magnitude larger than their ionospheric source.

Figures 2(a) and 2(b) show the electric and magnetic field wavelet spectrograms for the transverse wave fields. They are presented in a field-aligned coordinate system where in the magnetosphere **x** points approximately radially inwards from the magnetopause, **y** is close to the $\mathbf{Y}_{\mathrm{GSM}}$ direction [14], and **z** is in the direction of the dc field. The dc field goes through a ~180° rotation about the $\mathbf{Y}_{\mathrm{GSM}}$ direction when crossing the magnetopause so that on the magnetosheath side the **x** direction, in the field-aligned system, points approximately radially outwards. The E_x/B_y ratio calculated in this field-aligned system [2(c)] shows that an abrupt change occurs in the properties of these waves after 14:57:30 UT with the appearance of large fluxes of magnetosheath plasmas identified in Fig. 1.

Since the wave magnetic field amplitudes above 1 mHz are at least 3 times smaller than B_0, we derive a linear dispersion relation for drift-kinetic Alfvén waves [15] which arise because ions and electrons experience a diamagnetic drift across the density gradient shown in Fig. 1(b) given by

$$V_{dj} \approx \rho_j^2 \Omega_j |\nabla_x \ln(n_0)| \hat{y} \quad (1)$$

where $n_0 = n_0(x)$ is the density, $\Omega_j = q_j B_0/m_i$ the gyro-

 © 2005 The American Physical Society

frequency, and $\rho_j = (T_j/m_j)^{1/2}/\Omega_i$ the gyroradius. The gyro-averaged perpendicular ion drift for a wave with frequency $\omega \ll \Omega_i$ and perpendicular wave number k_y is given by $\mathbf{V}_{\perp i} = \mathbf{V}_{pi} + \mathbf{V}_{di} + \mathbf{V}_{E\times B}$ where

$$V_{pi} = \frac{m_i}{q_i B_0^2}\frac{dE_y}{dt}\hat{y} = -i\frac{\omega}{\Omega_i}\frac{\chi_i E_y}{B_0}\left(1-\frac{\omega_i^*}{\omega}\right)\hat{y} \qquad (2)$$

is the polarization drift and $V_{E\times B} = -[E_y I_0(\alpha_i)e^{-\alpha_i}/B_0]\hat{x}$. Here $\chi_i = [1 - I_0(\alpha_i)e^{-\alpha_i}]/\alpha_i$ and $I_0(\alpha_i)e^{-\alpha i}$ are finite gyroradii corrections [16] which become important when $\alpha_i = k_y^2\rho_i^2 \to 1$ where I_0 is the zero order modified Bessel function. The frequency of the ion drift wave is given by $\omega_i^* = k_y V_{di}$. The parallel ion drift is given by the parallel component of the ion momentum equation which in the linearized case for $v_i \ll \omega/k_\parallel \ll v_e$ becomes $V_{iz} = i\frac{q_i}{m_i\omega}[E_z I_0(\alpha_i)e^{-\alpha_i} + V_{di}B_x]$

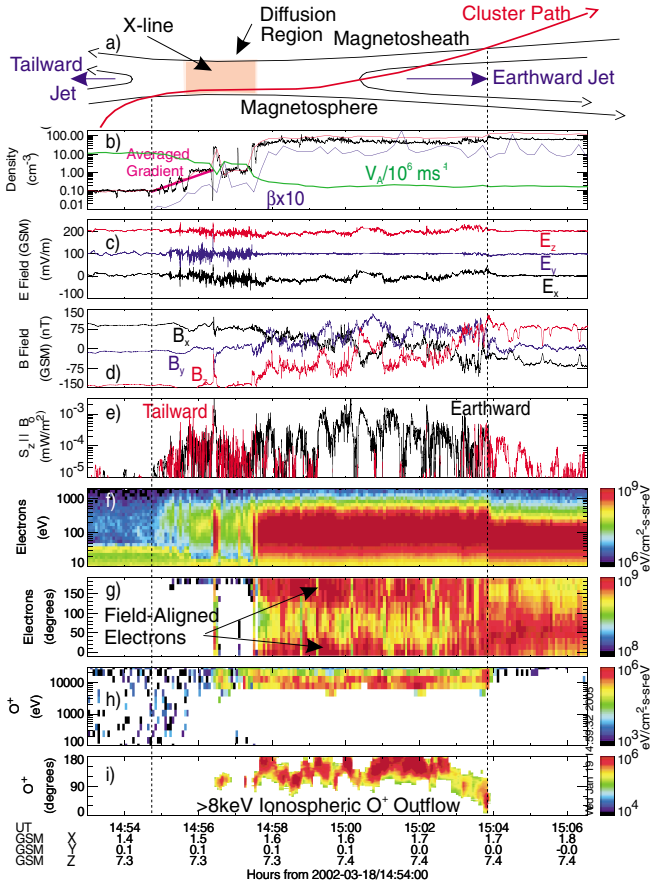

FIG. 1 (color). (a) Schematic of X line crossing; (b) Plasma density from ion spectrometer (red) and spacecraft potential (black) also shows the local Alfvén speed in ms^{-1} divided by 10^6 and plasma beta multiplied by 10 on the same scale; (c) Electric field in GSM coordinates under the assumption that $\mathbf{E}\cdot\mathbf{B}_0 = 0$ (y and z components have been shifted positive by 100 and 200 mV/m, respectively); (d) Magnetic field in GSM coordinates; (e) Field-aligned wave Poynting flux; (f) and (g) Electron energy flux and pitch angle spectra; (h) and (i) Oxygen ion pitch angle and energy spectra from Cluster 4. All data are from Cluster 3 unless otherwise stated.

where v_i and v_e are the ion and electron thermal speeds. Assuming $n_i = n_{io} + n_{i1}$ and substituting $V_{\perp i}$ and V_{iz} into the linearized ion continuity equation $\partial_t n_{i1} + n_{i0}\nabla\cdot V_i + V_i\nabla\cdot n_{i0} = 0$ we find

$$\frac{n_{i1}}{n_{i0}} = -i\frac{k_x}{\Omega_i}\frac{E_y}{B_0}\left[\chi_i\left(1-\frac{\omega_i^*}{\omega}\right) - \frac{I_0(\alpha_i)e^{-\alpha_i}}{k_y}\frac{\Omega_i}{\omega}|\nabla_x \ln(n_0)|\right] + i\frac{k_z\Omega_i}{\omega^2}\frac{E_z I_0(\alpha_i)e^{-\alpha_i}}{B_0}\left(1-\frac{\omega_i^*}{\omega}\right) \qquad (3)$$

where we have used the x component of Faraday's law to replace B_x. To determine the perturbed electron density we employ the parallel component of the electron momentum equation and by ignoring the electron polarization drift note that $V_{\rm ey} = V_{\rm de}$. Again replacing B_x using Faraday's law and taking $m_e \to 0$ this yields

$$\frac{n_{e1}}{n_{e0}} = -i\frac{q_e E_z}{k_z T_e}\left(1-\frac{\omega_e^*}{\omega}+\frac{\omega_e^*}{\omega}\frac{E_y}{E_z}\frac{k_z}{k_y}\right). \qquad (4)$$

For a quasineutral plasma we can equate (3) and (4) to provide the result

$$\frac{E_z}{E_y} = -\frac{k_z k_y \rho_s^2 \chi_i(1-\omega_i^*/\omega)}{1-\frac{\omega_e^*}{\omega}-I_0(\alpha_i)e^{-\alpha_i}\frac{k_z^2 V_s^2}{\omega^2}\left(1-\frac{\omega_i^*}{\omega}\right)} \qquad (5)$$

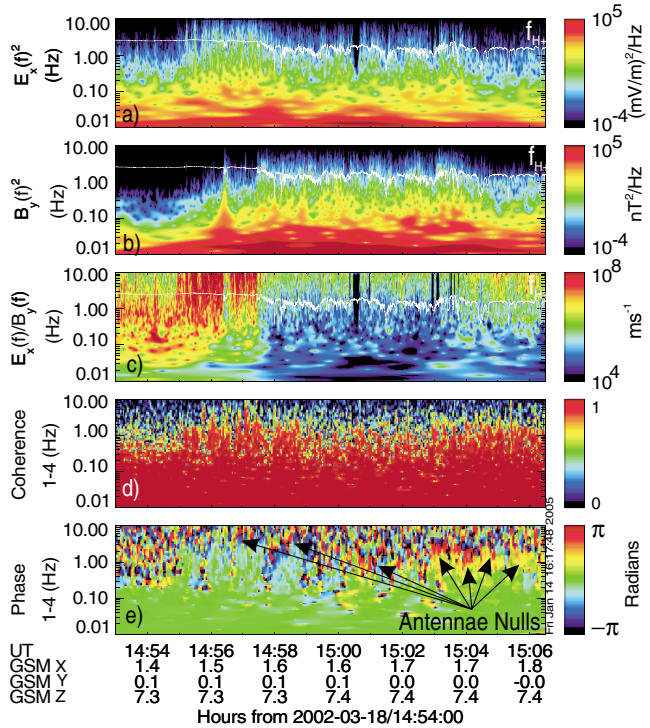

FIG. 2 (color). (a) E_x wavelet spectra; (b) B_y wavelet spectra; (c) E_x/B_y wavelet spectra; (d) two-point wavelet coherence between transverse B_y measurements from Cluster 1 and Cluster 4; (e) Phase difference between B_y measurements from Cluster 1 and Cluster 4. Coordinates are in the field-aligned system defined in the text.

where $V_s = (T_e/m_i)^{1/2}$ is the ion acoustic speed and $\rho_s = V_s/\Omega_i$ is the ion acoustic gyroradius. From the x component of Faraday's law we find $E_y/B_x = \omega/k_z[1 - k_y/k_z(E_z/E_y)]^{-1}$. Using this and the x component of Ampere's law $B_x = i\mu_0 J_y/k_z$ we obtain the dispersion relation,

$$k_z^2 v_A^2 k_y^2 \rho_s^2 \left(1 - \frac{\omega_i^*}{\omega}\right) = \left(\omega^2 - \omega_i^* \omega - \frac{k_z^2 v_A^2}{\chi_i}\right) \cdot \left[\left(1 - \frac{\omega_e^*}{\omega}\right) - \frac{k_z^2 V_s^2}{\omega^2} I_0(\alpha_i) e^{-\alpha_i} \left(1 - \frac{\omega_i^*}{\omega}\right)\right] \quad (6)$$

where we have used the substitution $J_y = -i\frac{\omega}{\mu_0 v_A^2}\chi_i E_y(1 - \omega_i^*/\omega)$ from (2). Subsequently, we can obtain the ratio of electric and magnetic fields as

$$\frac{E_y}{B_x} = \frac{\omega}{k_z}\left[1 + \frac{k_y^2 \rho_s^2 \chi_i (1 - \omega_i^*/\omega)}{1 - \frac{\omega_e^*}{\omega} - I_0(\alpha_i) e^{-\alpha_i} \frac{k_z^2 V_s^2}{\omega^2}(1 - \frac{\omega_i^*}{\omega})}\right]^{-1}. \quad (7)$$

These results are valid for $v_i \ll \omega/k_z \ll v_e$. Equation (7) is a new result not found elsewhere. We note that in the more general case where $k_\perp \cdot \nabla_\perp(\ln(n_0)) \neq 0$ then we can replace k_y with $k_\perp$ and ω_j^* with $k_\perp \cdot V_{dj}$. Using the Padé approximation $\chi_i = 1/(1 + \alpha_i)$ (5)–(7) reduce to the homogenous plasma result for the kinetic Alfvén wave [4] for $\omega/k_z \gg v_s$ and $\omega_i^* = \omega_e^* = 0$.

To compare the dispersion of the drift-kinetic wave derived above with the observations we determine $\mathbf{k}$ from the phase difference in magnetic field measurements between each of the four spacecraft. This is performed using a cross spectral technique [17] based on the wavelet transform by assuming a single wave mode. The phase difference between each spacecraft pair can be expressed as $\phi(\omega) = \phi_m(\omega) + n2\pi$ where $\phi_m(\omega)$ is the measured phase, ω is the frequency in the spacecraft frame, and $n = 0, \pm 1, \pm 2, \pm 3, \ldots$ is incremented by 1 whenever $\phi(\omega)$ passes through $\pm\pi$ (antennae null). This occurs when the distance between the two spacecraft or baseline length ($\sim$100 km) becomes equal to an odd multiple of 1/2 wavelengths projected along the vector separating the spacecraft. The occurrence of these nulls between spacecraft 1 and 4 can be identified in Figs. 2(d) and 2(e). These nulls allow us to resolve structures much less than the baseline length and down to an ion gyroradius ($\sim$ 30 km). From this measurement $\mathbf{k}(\omega)$ projected along the 1-4 baseline is then given by $k_{1\text{-}4}(\omega) = \mathbf{k} \cdot \mathbf{r}_{1\text{-}4}/r_{1\text{-}4} = \phi(\omega)/r_{1\text{-}4}$ where $\mathbf{r}_{1\text{-}4}$ is the vector pointing along the 1-4 baseline defined in this case in the geocentric solar magnetospheric (GSM) [14] coordinate system. Similar expressions can be written for each spacecraft pair or baseline so that with three baselines the full wave vector in GSM coordinates can be found from the solution of the equation $\mathbf{R}\mathbf{k}(\omega) = \mathbf{k}_R(\omega)$. Here $\mathbf{R}$ is a 3×3 matrix with each row defined by $\mathbf{r}_j/r_i$ where $\mathbf{r}_i$ is the vector pointing between each of the 3 spacecraft pairs and $\mathbf{k}_R(\omega) = (k_{1\text{-}4}, k_{2\text{-}3}, k_{2\text{-}4})$ is the wave vector in the nonorthogonal coordinate system defined by $\mathbf{R}$.

Figure 3(a) shows the wave vector determined in the manner just described using the spacecraft pairs 1-4, 2-3, and 2-4. The result is averaged over the interval from 14:55–14:56:30 UT and is in the field-aligned coordinate system defined above. This interval includes the reconnection X line and has been selected because of the density gradient it contains.

To solve the dispersion relation given by (6) we also require $|\nabla_y \ln(n_0)|$. This is determined from a cross-correlation analysis of the slow density and magnetic field variations (< 0.002 Hz) observed from each satellite. From this it is found that the density gradient points approximately radially outwards from the magnetopause and moves anti-sunward with the magnetopause along the spacecraft trajectory with a speed of $\sim$12 km/s. Given that the spacecraft speed at this time is $\sim$3 km/s sunward the density gradient from Fig. 1(c) averaged over 14:55–14:56:30 UT is $|\nabla_y \ln(n_0)| \approx 0.0034$ km^{-1}. This average gradient is indicated by the magenta line superimposed on the observed density gradient in Fig. 1(b) which shows that $n_0(x)$ over this interval varies exponentially as required for the validity of Eq. (6). With average ion and electron energies of 970 eV and 70 eV, respectively, an average density of 1.95 cm^{-3} and a gyrofrequency of $f_i = 2.4$ Hz we find from Eq. (1) that $V_{di} \approx 42.5$ kms^{-1} and

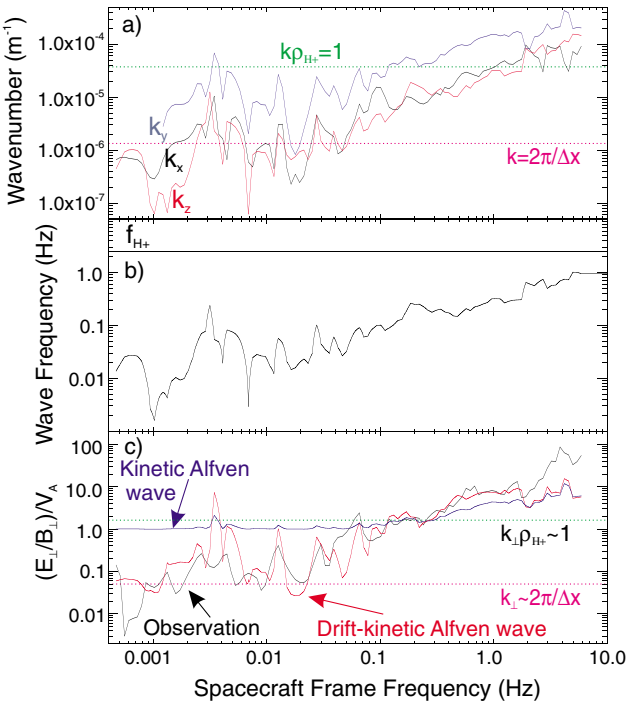

FIG. 3 (color). Averaged results from 14:55–14:56:30 UT; (a) Wave vector from interferometry in field-aligned coordinates as defined in the text; (b) Wave frequency for the drift-kinetic wave from the solution of Eq. (6); (c) Observed $E_\perp/B_\perp$ ratio (black), predicted result from the homogeneous theory (blue) and the predicted result from Eq. (7) (red).

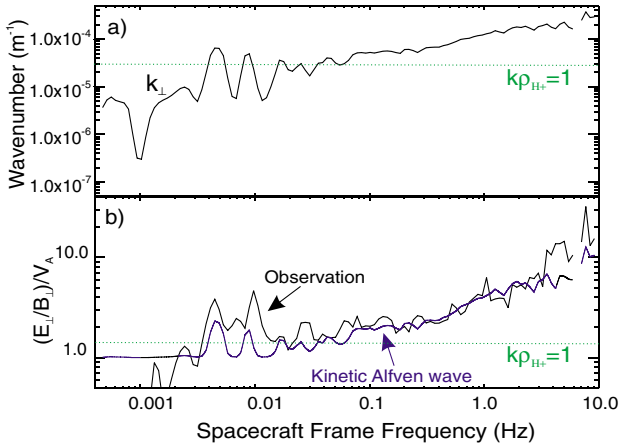

FIG. 4 (color). Average results from 14:58–15:04 UT; (a) Perpendicular wave number from interferometry; (b) Observed $E_\perp/B_\perp$ normalized by the local Alfvén speed (black) and the predicted result as described in the text (blue).

$V_{de} \approx 3.0$ kms^{-1}. Since $\mathbf{k}$ is known and $\omega_j^* = k_y V_{dj}$, Eq. (6) can now be solved for ω.

Figure 3(c) shows the observed $|E_\perp(\omega)/B_\perp(\omega)|$ ratio (where $E_\perp$ and $B_\perp$ are orthogonal) and the theoretical result from Eq. (7) using the drift-kinetic Alfvén wave solution of (6) shown in Fig. 3(b). The magenta and green horizontal lines show the strict range of validity for the model dispersion relation. This is bounded at the low frequency, or small $k_\perp$, end by the transverse width over which the model gradient is observed ($k_\perp = 2\pi/\Delta x$) and at the high frequency, or large $k_\perp$, end where $k_\perp \rho_{H+} = 1$, above which the finite gyroradii correction given by Eq. (7) becomes slightly inaccurate. Good agreement is found, however, between the observed and predicted ratios over the entire frequency range measured. We also have plotted the equivalent homogeneous result (blue curve, $|E_\perp(\omega)/B_\perp(\omega)| = v_A[1 + k_\perp(\omega)^2\rho_i^2]/[1 + k_\perp(\omega)^2 \times (\rho_i^2 + \rho_s^2)]^{1/2}$), which provides a comparatively poor estimate of the observed ratio. These results, while not conclusive, provide convincing evidence that the waves observed close to the reconnection X line are drift-kinetic Alfvén waves.

Figure 4(a) shows the wave vector averaged over the interval from 14:58–15:04:00 UT. This interval covers the entire width of the Earthward reconnection jet. In this case due to the high variability of the field-aligned direction it was not possible to determine a direction of $\mathbf{k}$ relative to $\mathbf{B}_0$ and so we only show the magnitude of $\mathbf{k}$. A negligible density gradient exists across this interval and so Eq. (6) reduces to the homogeneous case as given above and we assume $k_\perp \rightarrow k$. For an average ion temperature of 440 eV an electron temperature of 50 eV, an average density of 90 cm^{-3}, and a proton gyrofrequency of $f_i = 1.2$ Hz we have plotted the predicted $E_\perp/B_\perp$ ratio for the kinetic Alfvén wave over the observed value. These waves in the reconnection jet have the properties of kinetic Alfvén waves.

We have measured for the first time the wave vector of turbulence in the reconnection region. The drift-kinetic and kinetic Alfvén waves identified here are observed on both sides of the X line and propagate outwards from the reconnection site. Although this does not identify the mechanism which generates the waves, it clearly identifies reconnection as a source of kinetic Alfven waves. In the Earthward directed reconnection jet the observed wave Poynting flux shows that these waves travel towards the auroral ionosphere and may account for the Alfvén waves commonly observed there [4]. In the ionosphere they may also heat O^+ ions leading to ionospheric outflow [18] to account for the energetic 8–10 keV O^+ ions reported here at the magnetopause. These waves may also cause electron acceleration through the parallel electric field given by Eq. (5) to provide the field-aligned electron bursts in this event and those commonly found in the dayside auroral oval [11].

This research was supported by NASA Grants No. NAG5-12453, No. NAG5-12954, No. NAG5-12784, and No. FDNAG5-11944 and the Physics Department at the Chinese University of Hong Kong. C. C. is particularly indebted to Professor Chu Ming Chung for support while at CUHK and Charles Seyler and Jim McFadden for useful comments.

[1] J. W. Belcher and L. Davis Jr., J. Geophys. Res. **76**, 3534 (1971).
[2] A. C. Das and W.-H. Ip, Planet. Space Sci. **40**, 1499 (1992).
[3] J. R. Wygant *et al.*, J. Geophys. Res. **107**, 3 (2002).
[4] K. Stasiewicz *et al.*, Space Sci. Rev. **92**, 423 (2000).
[5] J. R. Stefant, Phys. Fluids **13**, 440 (1970).
[6] C. K. Goertz and R. W. Boswell, J. Geophys. Res. **84**, 7239 (1979).
[7] L. Chen, Z. Lin, and R. White, Phys. Plasmas **8**, 4713 (2001).
[8] S. R. Cranmer, G. B. Field, and J. L. Kohl, Astrophys. J. **518**, 937 (1999).
[9] R. J. Leamon *et al.*, Astrophys. J. **537**, 1054 (2000).
[10] A. Keiling *et al.*, Science **299**, 383 (2003).
[11] C. C. Chaston *et al.*, J. Geophys. Res. **108**, 8003 (2003).
[12] C. P. Escoubet *et al.*, Space Sci. Rev. **79**, 11 (1997).
[13] T. D. Phan *et al.*, Geophys. Res. Lett. **30**, 1509 (2003).
[14] C. T. Russell, Cosmic Electrodyn. **2**, 184 (1971).
[15] A. B. Mikhailovskii, in *Reviews of Plasma Physics*, edited by M. A. Leontovich (Consultants Bureau, New York, 1967), p. 159.
[16] C. Z. Cheng, J. Geophys. Res. **96**, 21159 (1991).
[17] J. Labelle and P. M. Kintner, Rev. Geophys. **27**, 495 (1989).
[18] C. C. Chaston *et al.*, J. Geophys. Res. **109**, A04205 (2004).